MATERIALS SCIENCE

Superconductivity across Lifshitz transition and anomalous insulating state in surface K–dosed $(Li_{0.8}Fe_{0.2}OH)FeSe$

Mingqiang Ren,[1] Yajun Yan,[1] Xiaohai Niu,[1] Ran Tao,[1] Die Hu,[1] Rui Peng,[1] Binping Xie,[1,2] Jun Zhao,[1,2] Tong Zhang,[1,2]* Dong-Lai Feng[1,2]*

In iron-based superconductors, understanding the relation between superconductivity and electronic structure upon doping is crucial for exploring the pairing mechanism. Recently, it was found that, in iron selenide (FeSe), enhanced superconductivity (T_c of more than 40 K) can be achieved via electron doping, with the Fermi surface only comprising M-centered electron pockets. By using surface K dosing, scanning tunneling microscopy/spectroscopy, and angle-resolved photoemission spectroscopy, we studied the electronic structure and superconductivity of $(Li_{0.8}Fe_{0.2}OH)FeSe$ in the deep electron-doped regime. We find that a Γ-centered electron band, which originally lies above the Fermi level (E_F), can be continuously tuned to cross E_F and contribute a new electron pocket at Γ. When this Lifshitz transition occurs, the superconductivity in the M-centered electron pocket is slightly suppressed, and a possible superconducting gap with a small size (up to ~5 meV) and a dome-like doping dependence is observed on the new Γ electron pocket. Upon further K dosing, the system eventually evolves into an insulating state. Our findings provide new clues to understand superconductivity versus Fermi surface topology and the correlation effect in FeSe-based superconductors.

INTRODUCTION

In high-T_c iron-based superconductors, carrier doping is one of the principal routes to induce superconductivity. Many factors, such as the density of states (DOSs), Fermi surface topology and nesting condition, and correlation strength, may vary significantly with carrier concentration. Detailed knowledge of the electronic structure versus doping is critical for understanding the pairing mechanism. Recently, it was found that through heavy electron doping, the T_c of FeSe can be enhanced from the bulk value of 8 K to more than 40 K. The doping can be achieved via interlayer intercalation [$A_xFe_{2-y}Se_2$ (A = K, Rb, …) (*1*, *2*), $(Li,NH_3)FeSe$ (*3*), $(Li_{1-y}Fe_xOH)FeSe$ (*4*)], interface charge transfer ($FeSe/SrTiO_3$) (*5*), surface K dosing (*6*), and ionic-liquid gating (*7*–*9*). Angle-resolved photoemission spectroscopy (ARPES) studies show that T_c enhancement in these systems is universally accompanied by a vanishing of the Γ hole pockets and that the superconducting gap on the M electron pockets is nodeless (*10*–*14*). Meanwhile, scanning tunneling microscopy (STM) studies suggest that the pairing symmetries of single-layer $FeSe/SrTiO_3$ and $(Li_{0.8}Fe_{0.2}OH)FeSe$ are plain s-wave (*15*, *16*), which differs from the $s_{\pm}$-wave of bulk FeSe and $FeTe_xSe_{1-x}$ (*17*, *18*), and that double-dome–like superconductivity is observed in FeSe films upon K dosing (*19*). These results indicate that the high-T_c phase in heavily electron-doped FeSe may be quite different from that in undoped FeSe, with changes in Fermi surface topology likely playing a crucial role.

Despite the T_c enhancement, the detailed phase diagram of electron-doped FeSe, particularly in the region beyond "optimal" doping, is still not fully understood. Recent ARPES results show that after FeSe films enter the high-T_c phase via surface K dosing, the electron correlation anomalously increases upon further doping, and eventually, an insulating phase emerges (*20*). This indicates remarkable complexity and new physics in the "overdoped" region. Here, by using low-temperature STM and ARPES, we studied the detailed evolution of the superconductivity and electronic structure of $(Li_{0.8}Fe_{0.2}OH)FeSe$ via surface K dosing. $(Li_{0.8}Fe_{0.2}OH)FeSe$ is already heavily electron-doped with a T_c of ~40 K (*4*, *16*). Surface K dosing can further increase the doping level of the surface FeSe layer. We observe that an unoccupied, Γ-centered electron band shifts significantly to the Fermi level (E_F) with increasing K coverage (K_c), whereas the double superconducting gap on M-centered electron pockets gets suppressed slightly. At certain K_c, the Γ-centered band crosses E_F, resulting in a Lifshitz transition of the Fermi surface. Shortly after the transition, a superconducting-like gap (up to 5 meV) opens at E_F, showing a dome-like dependence on K_c. This represents a new Fermi surface topology for iron-based superconductors, which has sizable electron Fermi pockets at both the Brillouin zone center and the zone corner. At even higher K_c, the system eventually evolves into an insulating phase, characterized by a large, asymmetric gap in excess of 50 meV. The presence of a novel Fermi surface topology, anomalous insulating phase, and the continuous tunability make $(Li_{0.8}Fe_{0.2}OH)FeSe$ a unique platform for gaining insight into the mechanism of iron-based superconductors.

RESULTS

Characterization of the as-cleaved FeSe surface

$(Li_{0.8}Fe_{0.2}OH)FeSe$ single crystals with a T_c of ~42 K (see fig. S1) were grown by hydrothermal reaction method (*4*, *21*). Details of the sample preparation and STM measurement are described in Materials and Methods. There are two possible surface terminations in a cleaved sample, namely, $Li_{0.8}Fe_{0.2}OH$-terminated and FeSe-terminated surfaces, as reported previously (*16*). Here, we focus on the FeSe surface with K dosing (see Materials and Methods for details). Figure 1A shows a topographic image of an as-cleaved FeSe surface. The square Se lattice (inset) and some dimer-shaped defects can be resolved. The dI/dV spectrum of this surface taken near E_F shows a double superconducting gap (Fig. 1B). For comparison, the topographic image

[1]State Key Laboratory of Surface Physics, Department of Physics, and Advanced Materials Laboratory, Fudan University, Shanghai 200433, China. [2]Collaborative Innovation Center of Advanced Microstructures, Nanjing 210093, China.
*Corresponding author. Email: tzhang18@fudan.edu.cn (T.Z.); dlfeng@fudan.edu.cn (D.-L.F.)

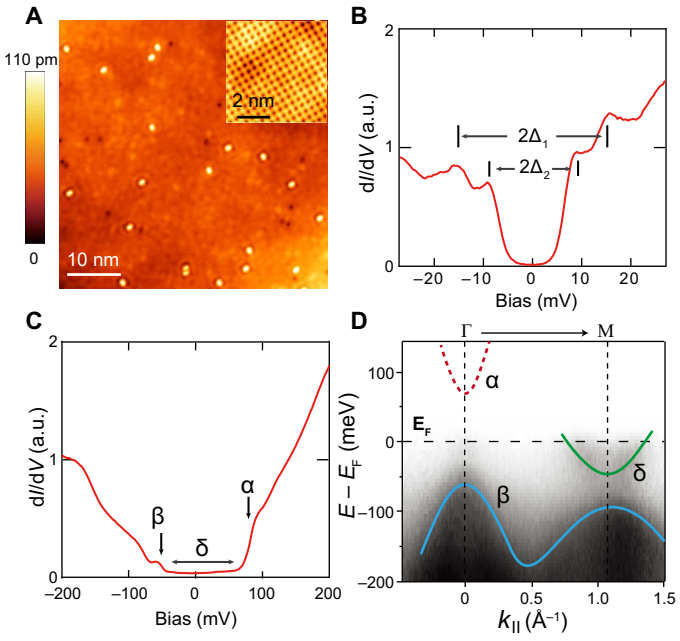

Fig. 1. Topographic image, tunneling, and ARPES spectra of as-cleaved ($Li_{0.8}Fe_{0.2}OH$)FeSe. (**A**) Topographic image of as-cleaved, FeSe-terminated surface (V_b = 100 mV and I = 50 pA); inset shows the surface lattice. (**B**) Low-energy dI/dV spectrum of as-cleaved FeSe surface, which displays double superconducting gaps of size Δ_1 = 15 meV and Δ_2 = 9 meV. a.u., arbitrary units. (**C**) Larger energy scale dI/dV spectrum. Arrows indicate the onset of the α and β bands (see text). Horizontal bar indicates the range of the δ band. (**D**) ARPES measurement of as-cleaved ($Li_{0.8}Fe_{0.2}OH$)FeSe. Solid curves track the dispersion of the β and δ bands, whereas the α band above E_F is sketched with red dashed curve.

and scanning tunneling spectroscopy (STS) of the $Li_{0.8}Fe_{0.2}OH$ surface are shown in fig. S2, which are distinct from the FeSe surface. The gap sizes of the FeSe surface determined from the two sets of coherence peaks are Δ_1 = 14.2 meV and Δ_2 = 8.9 meV, similar to previous reports (*16*, *22*). As shown by ARPES studies (*13*, *14*), these superconducting gaps are from M-centered electron pockets, whereas the double-peaked structure could be due to gap anisotropy (*23*) or band hybridization (*22*). The gap is found to be spatially homogeneous on the FeSe surface (see fig. S3), confirming the high quality of the sample.

Figure 1C shows the typical dI/dV spectrum of the FeSe surface on a larger energy scale (±200 meV). The tunneling conductance is relatively low near E_F but increases rapidly above 70 mV and below −55 mV. The double superconducting gap is not observable on this scale. We note that Huang *et al.* (*24*) observed similar dI/dV spectra in single-layer FeSe/$SrTiO_3$. They revealed that an unoccupied, Γ-centered electron band gives the steep dI/dV upturn at positive bias. This band is well reproduced in density functional theory (DFT) calculations (*24*, *25*). The dI/dV upturn at negative bias is from the onset of a Γ hole band below E_F. As explained by Huang *et al.* (*24*), the relatively low dI/dV near E_F is due to the M-centered electron bands (which dominate the DOS at E_F here) having a shorter decay length into the vacuum compared to Γ-centered bands, resulting in much lower tunneling probability. The ARPES data of as-cleaved ($Li_{0.8}Fe_{0.2}OH$)FeSe, as presented in Fig. 1D, display a similar band structure as single-layer FeSe/$SrTiO_3$. Hence, we would expect the resemblance in their tunneling spectra (on both FeSe surfaces). Below, we refer to the Γ-centered electron-like band as the α band, Γ-centered hole-like bands as β bands, and the M-centered electron-like band as the δ band.

Evolution of the electronic states after K dosing

Next, K atoms were deposited on the sample surface (see Materials and Methods for details). Figure 2 shows typical topographic images of the FeSe surface with K_c from 0.008 to 0.306 ML. Here, we define one monolayer (ML) as the areal density of Fe atoms in single-layer FeSe (1.41×10^{15}/cm^2). At small K_c, K atoms are randomly distributed on the surface (Fig. 2, A and B). At certain coverages like 0.098 and 0.124 ML, K atoms can form locally ordered structures, such as $\sqrt{5} \times \sqrt{5}$ [with respect to the FeSe unit cell (UC); Fig. 2C], or a sixfold close-packed lattice with an inter-atom spacing of 0.78 nm (Fig. 2D; see also fig. S4A). There are different rotational domains observed in Fig. 2D (as marked by the arrows) because of the different symmetry of the K lattice and underlying FeSe lattice. When $K_c > 0.15$ ML, K atoms begin to form clusters, and no ordered surface structures can be observed (see fig. S4, C and D, for larger-scale images).

Figure 3 (A and B) shows the detailed evolution of the dI/dV spectra as a function of K_c. At low coverage (K_c < 0.080 ML), it is seen from Fig. 3A that the onset of the α band gradually moves to lower energy. However, the β band does not shift together with α, instead moving slightly to higher energy. This anomalous behavior is possibly due to correlation effects in FeSe (*20*). In Fig. 3B, one sees that double superconducting gaps barely change at $K_c \leq 0.048$ ML. When K_c reaches 0.062 to 0.075 ML, the bottom of the α band approaches E_F; thus, the corresponding spectra in Fig. 3B tilt up at positive bias. However, the double coherence peaks at negative bias are still observable, which indicates that the gap on the δ band still exists. The corresponding gap size is only slightly suppressed (Δ_1 = 13.9 meV and Δ_2 = 8.6 meV at K_c = 0.075 ML). This indicates that the superconductivity in the δ band is only weakly sensitive to additional electron doping.

When K_c reaches 0.080 ML, the α band begins to cross E_F, as seen in Fig. 3 (A and B). The tunneling conductance near E_F is now greatly enhanced and dominated by the α band. The spectral weight from the δ band is overwhelmed, and the double coherence peaks are no longer observable (note that the normalization scheme of Fig. 3B changes at this point to make all spectra appear with a similar scale; see fig. S5 for unnormalized dI/dV spectra near this Lifshitz transition). There is no gap-like feature near E_F at K_c = 0.080 or 0.098 ML, or the gap is much smaller than our experimental resolution (~1 meV). This indicates that the pairing is weak on the α band as it crosses E_F. In Fig. 4A, we summarize the energy shifts of the α and β bands as a function of K_c, by tracing the band bottom or top. We note that the sensitivity of the band position of α to surface K dosing is consistent with recent DFT calculations (*25*). It was shown that the α band has both Se 4*p* and Fe 3*d* orbital characters, which makes it sensitive to Fe-Se distance or Se height (h_{Se}) (*24*). K dosing could significantly affect the h_{Se} of the surface Se layer.

The Fermi surface of α will be a new electron pocket at Γ. To look for this pocket, we performed quasi-particle interference (QPI) mapping at K_c = 0.124 ML. As shown in Fig. 2D, for this coverage, the K atoms form a close-packed structure with a relatively smooth, ordered surface, which is suitable for QPI measurements. The mapping was carried out in an area of 100 × 100 nm^2 (Fig. 5A). Figure 5 (B and C) shows a typical dI/dV map taken at V_b = 10 mV and its fast Fourier transform (FFT). A complete set of dI/dV maps and FFTs taken within ±50 mV of E_F can be found in fig. S6. All FFTs display an isotropic scattering ring centered at q = (0, 0), with the radius increasing with energy. In Fig. 5D, we summarize the FFT linecuts through the center of the scattering ring, taken at various

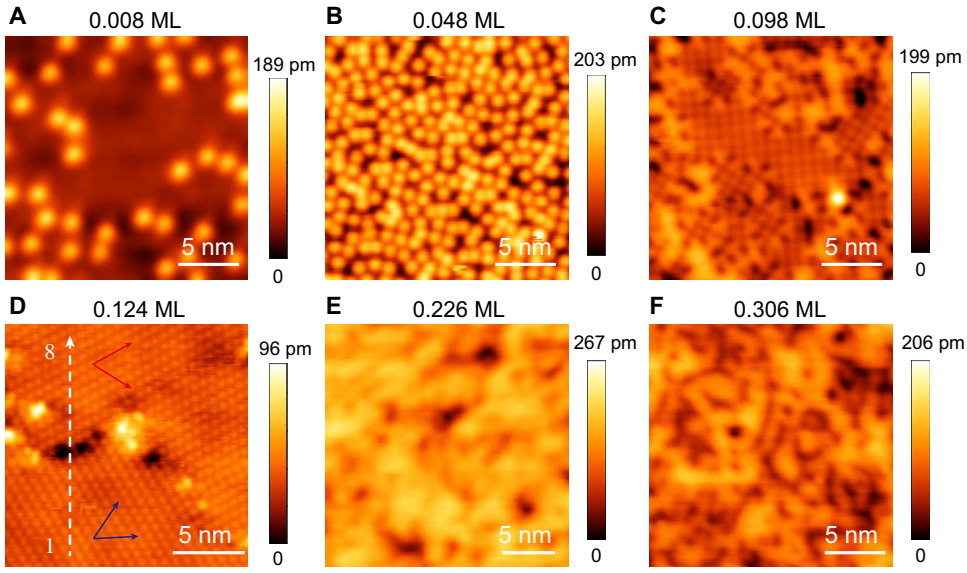

Fig. 2. Topographic images of the FeSe surface with a different K_c. (**A**) K_c = 0.008 ML. (**B**) K_c = 0.048 ML. (**C**) K_c = 0.098 ML. (**D**) K_c = 0.124 ML. (**E**) K_c = 0.226 ML. (**F**) K_c = 0.306 ML. Typical imaging parameters are V_b = 0.5 V and I = 50 pA. The red and blue arrows in (D) indicate the orientation of two different rotational domains. The white dashed arrow marks the position where the STS in Fig. 5E is taken.

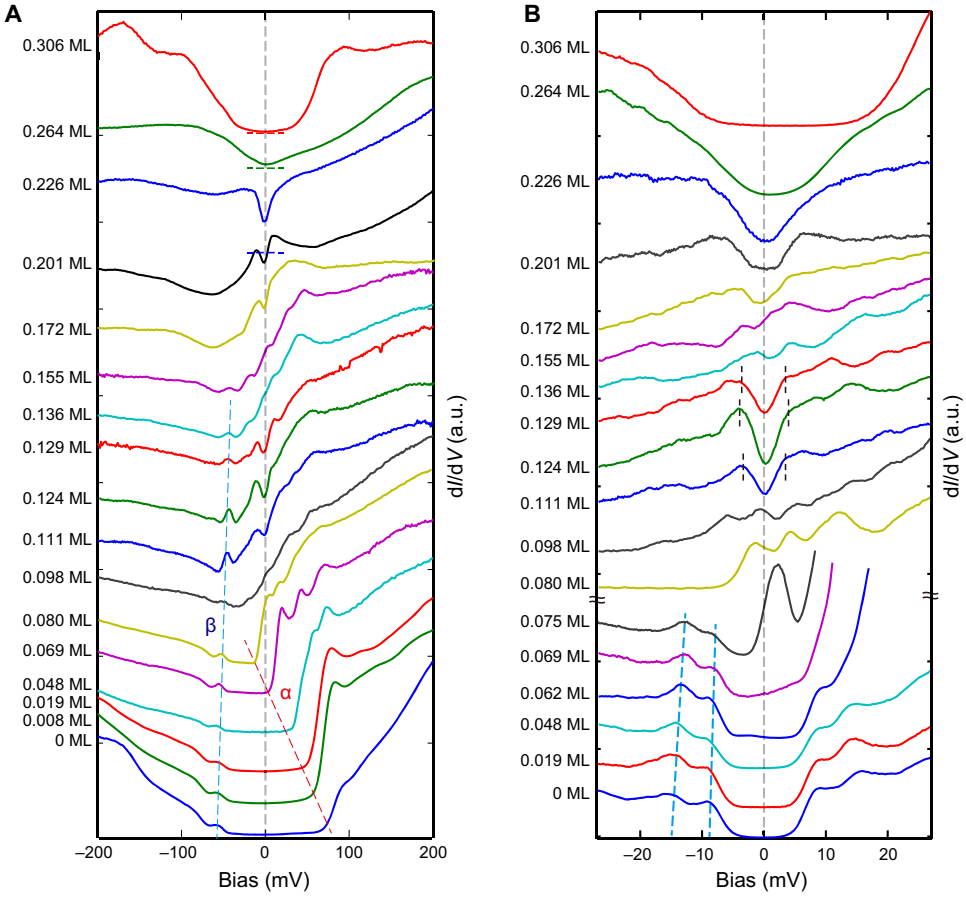

Fig. 3. Evolution of d*I*/d*V* spectra taken on the FeSe surface with various K_c as labeled. (**A**) Typical d*I*/d*V* spectra taken within large energy range (±200 meV). Red and blue dashed lines track the onsets of the α and β bands. The zero positions of the spectra at K_c = 0.306, 0.264, and 0.226 ML are marked by short horizontal bars. (**B**) Typical d*I*/d*V* spectra taken near E_F (±27 meV). Two blue dashed lines track the superconducting coherence peaks at negative bias. The curves at $K_c \leq 0.075$ ML are normalized by the d*I*/d*V* value at V_b = −27 mV, and the curves at $K_c > 0.075$ ML are normalized by the value at V_b = 27 mV. E_F (V_b = 0) is indicated by gray dashed lines. At K_c = 0.111, 0.124, and 0.129 ML, the gap edge positions (defined as Δ_3) are marked by short dashed lines.

energies. An electron-like dispersion can be clearly seen, which is fully consistent with the presence of the α band. By assuming $q = 2k$ for the intraband backscattering condition, a parabolic fit yields the Fermi crossing at $k_F = 0.075$ Å^{-1} and the band bottom at −37 meV (this value is also marked in Fig. 4A). Such a sizable electron pocket has not been observed before in iron-based superconductors at the Γ point [for comparison, the k_F of δ band for $(Li_{0.8}Fe_{0.2}OH)FeSe$ is 0.21 Å^{-1} at $K_c = 0$; see the study of Yan *et al.* (*16*)].

Shortly after the α band begins being occupied, starting from K_c = 0.111 ML, one sees a small gap open at E_F. We define the gap size by the peak or kinks on the gap edge and refer it to Δ_3 below. Δ_3 reaches 3.5 to 4 meV at $K_c = 0.124$ ML and closes at about $K_c = 0.136$ ML. In Fig. 5E, we show an STS linecut taken on the surface in Fig. 2D (K_c = 0.124 ML)—the small gap is spatially uniform, with coherence peaks in most locations. We have checked this gap in several different samples and found that it can reach ~5 meV at the optimal K_c near 0.12 ML. Figure 5F shows the temperature dependence of the gap at the optimal K_c, with clearly defined coherence peaks. It becomes less prominent as the temperature increases, vanishing at $T = 35$ K, close to the bulk T_c of the sample (~42 K). Therefore, it is likely that a possible superconducting gap opens on the α band, having a dome-like doping dependence. There could be other possibilities such as a charge density wave–induced gap; however, we did not observe any additional spatial modulation in the topographic image (Fig. 2D and fig. S4A), QPI maps (Fig. 5 and fig. S6), and their FFTs (fig. S4B). The gap has significant nonzero dI/dV at $V_b = 0$, which could be due to gap anisotropy and/or thermal broadening effects. Measurements at lower temperature and high magnetic field would further clarify the nature of this gap.

The small gap disappears at K_c = 0.136 and 0.155 ML, but starting from K_c = 0.172 ML, another gap-like feature develops at E_F. This time, the gap size keeps increasing upon further K dosing, and eventually at K_c = 0. 306 ML, it exceeds 50 meV in width with a nearly flat bottom (Fig. 3B). We note that at K_c = 0.201 or 0.226 ML, the gap has a comparable size with the possible superconducting gap (Δ_3) at $K_c = 0.124$ ML, but the feature is broader (bigger than Δ_3 with weak or no coherence peak). Furthermore, at $K_c = 0.306$ ML, the gap is asymmetric with respect to E_F, and STM imaging is not possible for bias voltages inside the gap. Therefore, the gap opening starting from K_c = 0.172 ML likely evidences that the system enters an insulating state, with gradually depleted DOS at E_F. To illustrate this more quantitatively, in Fig. 4B, we integrated the dI/dV values extracted from Fig. 3A over the bias range of ±8 meV, as a function of K_c (>0.1 ML). This will give an estimation of the DOS of the α band near E_F (note that the integration window is larger than Δ_3). It is clear that when $K_c < 0.172$ ML, the DOS increases with K_c, although it quickly drops thereafter, indicating a metal-insulator transition.

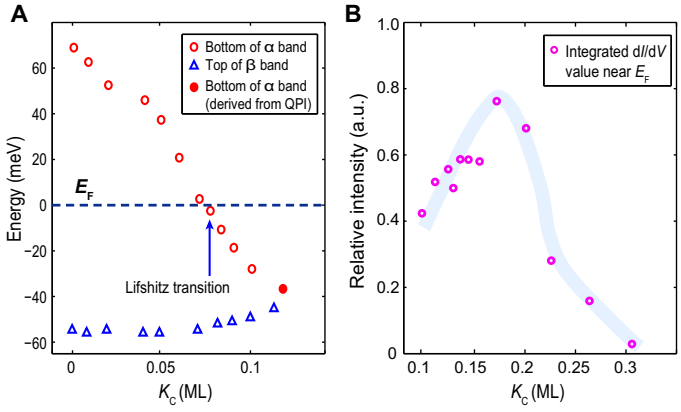

Fig. 4. Doping dependence of the energy band position and the DOS near E_F. (**A**) The doping dependence of the band bottom (top) energy of the α (β) band. At $K_c = 0.080$ ML, the α band begins to cross E_F. (**B**) Integrated dI/dV values within the bias range of ±8 meV as a function of K_c, which reflects the DOS near E_F.

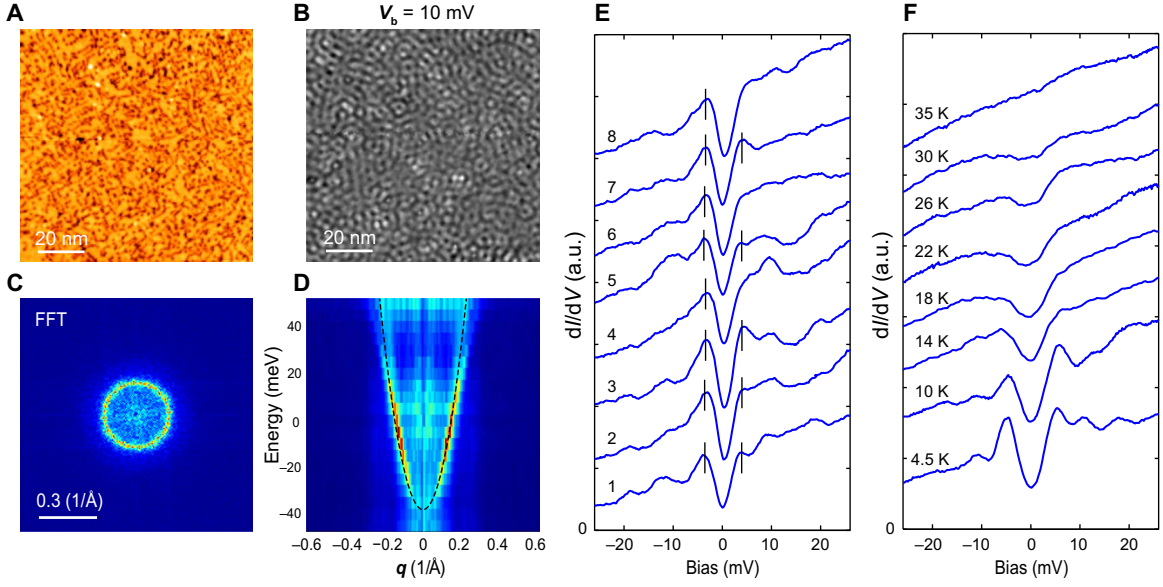

Fig. 5. QPI measurement of the α band and the spatial and temperature dependence of its gap. (**A**) Topographic image of the mapping area of size 100 × 100 nm^2 ($K_c = 0.124$ ML). (**B**) Typical dI/dV map taken at $V_b = 10$ mV. The set point for dI/dV map is as follows: $V_b = 50$ mV, $I = 150$ pA, and $\Delta V = 3$ mV. (**C**) FFT image of (B). (**D**) Intensity plot of the FFT linecuts through $q = (0, 0)$; dashed curve is the parabolic fit. Note that the small gap is not observable here because of the large modulation (ΔV). (**E**) A dI/dV linecut taken along the dashed arrow in Fig. 2D, showing a spatially uniform gap. Bars indicate the coherence peaks. (**F**) Temperature dependence of the gap taken on a different sample with K_c ~ 0.12 ML.

This finding is consistent with the insulating state observed in K-dosed FeSe films by ARPES (*20*) and in ionic liquid–gated ($Li_{1-x}Fe_xOH$)FeSe (*26*). Note that the topographic image of K_c = 0.306 ML in Fig. 2F and fig.S4D only shows a disordered structure. This suggests that the insulating phase is not due to the formation of some impurity phase (such as $K_2Fe_4Se_5$) but is intrinsic to deeply electron-doped FeSe. Moreover, the emergence of the insulating phase also indicates that K atoms do not form a surface metallic layer by themselves up to K_c = 0.306 ML. The STS in Fig. 3 will reflect the electron states of doped FeSe layer.

To facilitate the understanding of the STM data, we performed ARPES measurements on K-dosed ($Li_{0.8}Fe_{0.2}OH$)FeSe (experiment details are described in Materials and Methods). Figure 6 (A and B) shows ARPES intensity along the cuts crossing Γ and M (Fig. 6C) as the function of K_c. Note that the K_c here is estimated from K flux and deposition time (*t*) (see Materials and Methods). As seen in Fig. 6B, the size of the δ Fermi pocket increases with K dosing (at $K_c \leq$ ~0.27 ML), indicating the electron doping. Meanwhile, near the Γ point (Fig. 6A), there is a noticeable spectral intensity that shows up and increases near E_F upon K dosing (at $K_c <$ ~0.27 ML). To illustrate it more quantitatively, we plot the corresponding momentum distribution curve (MDC) and energy distribution curve (EDC) (taken near E_F and k = 0) for various K_c in Fig. 6 (D and E) (see figure captions). The spectral intensity at Γ evidences the emergence of an electron pocket, although the band dispersion is not clear, which could be due to small pocket size and/or limited resolution here. To have a comparison with the STM result, in the K_c ~ 0.12 ML panel of Fig. 6A, we superposed the band dispersion of α, which is derived from the QPI of K_c = 0.124 ML (Fig. 5D). There is a qualitative match between QPI band dispersion and ARPES intensity at Γ. Furthermore, it is notable that at high dosing (K_c ~ 0.45 ML and t = 302 s), the bands at both Γ and M near E_F became unresolvable, which is also consistent with a metal-insulator transition suggested by the STM data. In Fig. 6F, we show symmetrized EDC taken near the k_F of the δ band (marked in Fig. 6B), which displays the evolution of the superconducting gap on the δ band. The gap size was ~13 meV at K_c = 0 and ~0.06 ML, which decreased to ~9 meV at K_c ~ 0.12 ML and disappeared at K_c ~ 0.27 ML. The disappearance of superconductivity on the δ band before entering the insulating phase is also observed in K-dosed FeSe films (*20*).

We noted that the ARPES signal should come from both FeSe and $Li_{0.8}Fe_{0.2}OH$ surfaces (the light spot is of millimeter size here). Our

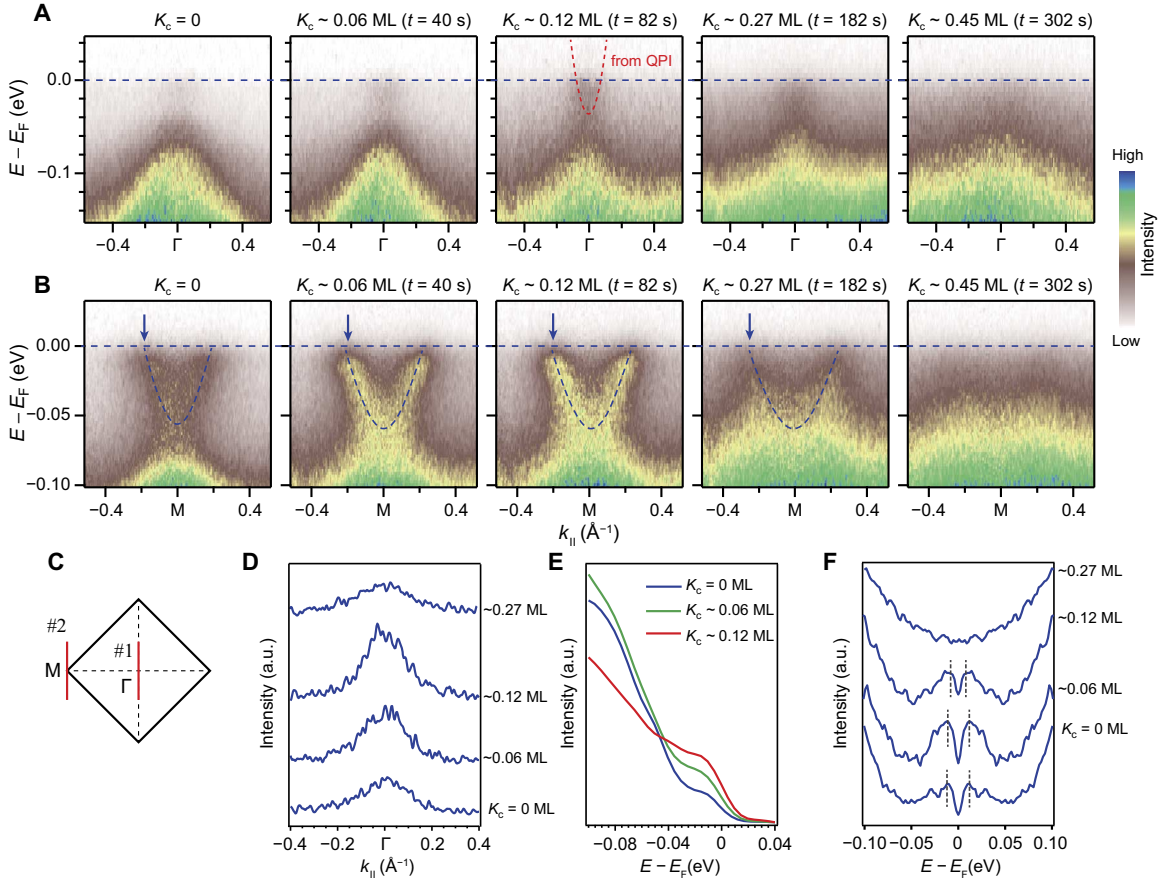

Fig. 6. ARPES measurement of the band structure of surface K–dosed ($Li_{0.8}Fe_{0.2}OH$)FeSe. (**A**) ARPES intensity along cut #1 shown in (C), as a function of K_c and deposition time (*t*). Red dashed line in the third panel (K_c ~ 0.12 ML) represents the band dispersion of α that derived from QPI (Fig. 5D). (**B**) ARPES intensity along cut #2 shown in (C), as a function of K_c and *t*. Dashed lines track the dispersion of the δ band. (**C**) Sketch of the Brillouin zone of ($Li_{0.8}Fe_{0.2}OH$)FeSe. (**D**) Evolution of the MDC along cut #1 upon K dosing, integrated over ±14 meV at E_F (curves are shifted vertically for clarity). The intensity at Γ increases up to K_c ~ 0.12 ML. The decreased intensity at K_c ~ 0.27 ML could be due to approaching to the insulating phase (consistent with Fig. 4B). (**E**) Evolution of the EDC taken around k = 0 (Γ point) upon K dosing (K_c = 0 to 0.12 ML). The increased intensity between −0.04 and 0 eV is consistent with the emergence of an electron pocket. (**F**) Symmetrized EDC showing the evolution of the superconducting gap on the δ band, as a function of K_c. The momenta of individual spectra are indicated by the arrows in (B).

previous STM study found a small electron pocket at Γ for the $Li_{0.8}Fe_{0.2}OH$ surface (*16*), and it may account for the weak spectral weight at Γ near E_F for the $K_c = 0$ case in Fig. 6A (also indicated in Fig. 6, D and E). We note that a recent μSR (muon spin spectroscopy) study reported proximity-induced superconducting gap in the $Li_{1-x}Fe_xOH$ layers, which also suggest that the $Li_{1-x}Fe_xOH$ layer is conductive (*27*).

Figure 7 summarizes the observed electronic states from the STS in Fig. 3, as a function of K_c. This phenomenological phase diagram contains four distinct regimes. In regime I ($0 \le K_c \le 0.075$ ML), the Fermi surface only comprises the M-centered δ band, and its superconducting gap (Δ_1 and Δ_2) is only gradually suppressed. In regime II (0.080 ML $\le K_c \le$ 0.172 ML), the α band crosses E_F, introducing a new electron pocket at Γ (illustrated in the inset). A possible new superconducting dome on the α band exists in the middle of this regime (green squares represent the gap size of Δ_3). As a complement, the ARPES measured gap sizes on the δ band (from Fig. 6F) are also marked here by gray circles. It appears that the gap persists in the left part of regime II; thus, STM measured Δ_1 and Δ_2 should also extend to regime II (indicated by two short dashed lines). In regime III (0.172 ML $< K_c \le$ 0.26 ML), the DOS near E_F begins to decrease as the system approaches a metal-insulator transition. Finally, in regime IV ($K_c >$ 0.26 ML), the DOS near E_F is depleted, and the system enters an insulating state.

We noted that the Fermi surface of $A_xFe_{2-y}Se_2$ at the $k_z = \pi$ plane (*10*) is similar to the one shown in regime II of Fig. 7. However, the center electron pocket does not exist at Γ ($k_z = 0$) in $A_xFe_{2-y}Se_2$, reflecting its significant three-dimensional (3D) character. In $(Li_{0.8}Fe_{0.2}OH)FeSe$, the interlayer spacing between two FeSe layers (~0.932 nm) (*4*) is significantly larger than that of $A_xFe_{2-y}Se_2$ (~0.702 nm) (*1*). This makes the Fermi surface of $(Li_{0.8}Fe_{0.2}OH)FeSe$ rather 2D (*14*).

DISCUSSION

Surface K–dosed $(Li_{0.8}Fe_{0.2}OH)FeSe$ provides several unique opportunities to understand superconductivity in Fe-based superconductors. First, the emergence of the Γ-centered electron pocket will introduce a new pairing channel. For most known iron-based superconductors, there are two typical types of Fermi surface topology: one with hole pockets at the zone center and electron pockets at the zone corner and the other with only electron pockets at the zone corner. The scattering between different Fermi pockets has direct consequences on the pairing symmetry (*28*–*31*). It was suggested that the interband interactions (spin fluctuations) between the Γ-hole and M-electron pockets with wave vector $\mathbf{Q} = (\pi, 0)$ are the main pairing glue, which will lead to $s_{\pm}$-wave pairing symmetry (*28*, *29*). However, the absence of a Γ pocket in electron-doped FeSe-based systems seriously challenges this scenario. Later, it was suggested that the interaction between neighboring M-electron pockets with $\mathbf{Q} = (\pi, \pi)$ would dominate pairing in these cases and lead to a d-wave pairing symmetry (*29*–*31*), but this picture lacks direct experimental support. Recently, some theoretical work shows that the "incipient" band (a band that is close to but does not cross E_F) may still play an important role in pairing, with a significant pairing potential (*32*–*34*), and a large "shadow gap" feature was observed in the incipient Γ band in $LiFe_{1-x}Co_xAs$ (*35*). Here, by surface K dosing $(Li_{0.8}Fe_{0.2}OH)FeSe$, we are able to continuously tune the α band to approach and cross E_F, which is expected to enable the interaction between two electron bands at Γ and M with $\mathbf{Q}$ near (π, 0) (for $A_xFe_{2-y}Se_2$, these interactions may exist but would be weakened by the strong 3D character of its central electron pocket, as aforementioned). We did not observe gap opening on the α band near its Lifshitz transition (0.062 ML $\le K_c \le$ 0.098 ML), although the gap on the δ band is slightly suppressed. This would suggest that such a Γ-M interaction does not promote superconductivity at the onset of the transition and that the dominant pairing interaction must still lie in the δ band. When the α band does develop a gap in regime II, assuming that the observed gap is possibly a superconducting gap, the small gap size (compared to that on the δ band) also suggests a weak pairing potential on the α band. Because the gap-closing temperature is quite high, this gap could be induced by the δ band through normal interband scattering, as the latter band remains superconducting, as indicated in Figs. 6F and 7. Nevertheless, the dome-like behavior suggests that the α band gradually participates in the pairing. Because of the close competition of various pairing channels, the new type of Fermi surface topology found here may help facilitate a novel superconducting pairing state. In addition, orbital-selective pairing (*36*, *37*), as recently evidenced in bulk FeSe (*38*), may also relate to our results. Band calculation of single-layer FeSe shows that the major orbital component of α is d_{x2-y2} (*24*), which differs from the d_{xy} and d_{xz}/d_{yz} orbitals that comprise the δ band (*29*). Further theoretical work considering all possible inter- and intraband interactions and orbital structures will be needed to understand the electron pairing in such a case.

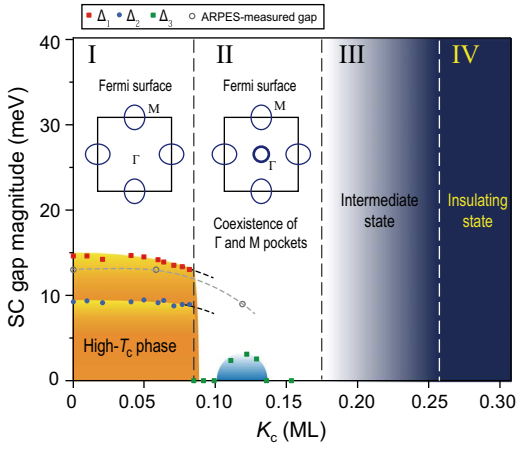

Fig. 7. Summarized phase diagram of surface K–dosed $(Li_{0.8}Fe_{0.2}OH)FeSe$. The insets in regimes I and II sketch the Fermi surface before and after the Lifshitz transition. The red, blue, and green dots represent the value of Δ_1, Δ_2, and Δ_3, respectively. Gray circles represent the ARPES measured gap size on the δ band (gray dashed line traces its variation). ARPES measurement suggests that Δ_1 and Δ_2 would not suddenly disappear when entering regime II, as illustrated by the short black dashed lines. SC, superconducting.

Second, the metal-insulator transition observed here provides more clues as to the unusual doping-driven insulating phase in FeSe. In particular, our result shows that the DOS near E_F is gradually depleted during the transition, over a relatively wide doping range (from K_c = 0.172 to ~0.26 ML). This differs from transport measurements in ionic liquid–gated $(Li_{1-x}Fe_xOH)FeSe$, where a sharp, first-order–like transition is observed (*26*). The smooth transition is consistent with the ARPES result on K-dosed FeSe, where a gradual suppression of spectral weight accompanied by an increasing effective mass is observed (*20*), suggesting a correlation-driven transition (*39*). We note that a similar insulating phase has been observed in $Rb_xFe_{2-y}Se_{2-z}Te_z$ (*40*), which indicates that the correlation-driven metal-insulator transition might be universal in FeSe-derived superconductors.

Third, K dosing may be able to change the band topology of the top FeSe layer, inducing a topological phase transition. Recently, Wu *et al.* (*41*) proposed that the band topology of the Fe(Te)Se system is controlled by Se(Te) height, which affects the separation (Δ_n) between the electron and hole bands at Γ, and suggested that if Δ_n is smaller than 80 meV, then spin-orbit coupling can induce band inversion and lead to a nontrivial Z_2 topology. In our case, the separation between the α and β bands is continuously reduced from 120 meV (K_c = 0) to ~20 meV (K_c ~ 0.1 ML), as summarized in Fig. 4A. Therefore, such a topological phase transition may well be achievable. We noted that at K_c > 0.1 ML, the evolution of the α and β bands is hard to identify in STS (Fig. 3A); however, topological edge states may exist near step edges if the system enters a nontrivial phase, which deserves further investigation.

In summary, by dosing K on the surface of $(Li_{0.8}Fe_{0.2}OH)FeSe$, a new electron pocket can be introduced at the Γ point. This Lifshitz transition creates a new type of Fermi surface topology and enables a new pairing channel via Γ-M interactions. However, only a small gap feature was observed on the new Γ pocket, indicating its weak pairing potential. Further doping eventually drives the system into an anomalous insulating state. In addition, nontrivial band topology might be realized by the K dosing–induced band shift. This singular combination of new opportunities makes K-dosed $(Li_{0.8}Fe_{0.2}OH)FeSe$ an intriguing platform for studying the pairing interaction, correlation effects, and topological properties in iron-based superconductors.

Upon completing this work, we noticed an ARPES study on surface K–dosed 1-UC FeSe/$SrTiO_3$ (*42*), which has similar band structure as $(Li_{0.8}Fe_{0.2}OH)FeSe$. An electron pocket at Γ is also observed after K dosing. This suggests the broader applicability of our findings.

MATERIALS AND METHODS

Sample growth

$(Li_{0.8}Fe_{0.2}OH)FeSe$ single crystals were grown by hydrothermal ion-exchange method described by Dong *et al.* (*21*). $K_{0.8}Fe_{1.6}Se_2$ matrix crystal, $LiOH{\cdot}H_2O$, Fe, and CH_4N_2Se were used as starting materials. During the hydrothermal reaction, $Li_{1-x}Fe_xOH$ layers were formed and replaced the K atoms in $K_{0.8}Fe_{1.6}Se_2$ (*21*). Resistivity and magnetic susceptibility measurements (fig. S1, A and B) confirm the T_c of about 42 K. The optical image (fig. S1C) shows that the sample surface is composed of separated domains with the size of tens of micrometers. This morphology may be due to the ion-exchange process.

STM measurement

STM experiment was conducted in a commercial CreaTec STM at the temperature of 4.5 K. $(Li_{0.8}Fe_{0.2}OH)FeSe$ samples were cleaved in ultrahigh vacuum at 78 K. Pt tips were used in all measurements after careful treatment on a Au(111) surface. The tunneling spectroscopy (dI/dV) was performed using a standard lock-in technique with modulation frequency f = 915 Hz and typical amplitude ΔV = 1 mV.

ARPES measurement

ARPES measurement was conducted in an in-house ARPES system with a helium discharge lamp (21.2-eV photons), at the temperature of 11 K, using Scienta R4000 electron analyzers. The energy resolution was 8 meV, and the angular resolution was 0.3°. $(Li_{0.8}Fe_{0.2}OH)FeSe$ samples were cleaved in situ under ultrahigh vacuum. During measurements, the spectroscopy qualities were carefully monitored to avoid the sample aging issue.

K dosing

K atoms were evaporated from a standard SAES alkali metal dispenser, and the samples were kept at 80 K during K dosing. In the STM study, the K_c at low coverages was obtained by directly counting surface K atoms. Then, the K deposition rate was carefully calibrated, and the K_c at high coverage was calculated by deposition rate and time. The K_c dependence of the STS was obtained by repeated deposition of K atoms on one sample. After each deposition, the STM tip was nearly placed on the same surface domain, which is found to be mostly covered by the FeSe-terminated surface. In the ARPES study, K_c was estimated from the K flux rate (measured by a quartz crystal microbalance) and deposition time. K_c dependence of the ARPES spectra was obtained by repeated deposition of K atoms on one sample.

SUPPLEMENTARY MATERIALS

Supplementary material for this article is available at http://advances.sciencemag.org/cgi/content/full/3/7/e1603238/DC1

fig. S1. Resistivity, dc magnetic susceptibility measurement, and optical microscopy image of $(Li_{0.8}Fe_{0.2})OHFeSe$ single crystal.

fig. S2. Topographic image and STS taken on the as-cleaved $Li_{0.8}Fe_{0.2}OH$ surface.

fig. S3. Spatial distribution of the superconducting gap on the as-cleaved FeSe surface.

fig. S4. Additional topographic images of the FeSe surface after K dosing.

fig. S5. Unnormalized dI/dV spectra at the K_c near Lifshitz transition.

fig. S6. dI/dV maps and corresponding FFTs taken in an area of 100 × 100 nm^2 of the FeSe-terminated surface at K_c = 0.124 ML.

REFERENCES AND NOTES

1. J. Guo, S. Jin, G. Wang, S. Wang, K. Zhu, T. Zhou, M. He, X. Chen, Superconductivity in the iron selenide $K_xFe_2Se_2$ ($0 \le x \le 1.0$). *Phys. Rev. B* **82**, 180520(R) (2010).
2. A. F. Wang, J. J. Ying, Y. J. Yan, R. Liu, X. G. Luo, Z. Y. Li, X. F. Wang, M. Zhang, G. J. Ye, P. Cheng, Z. J. Xiang, X. H. Chen, Superconductivity at 32 K in single-crystalline $Rb_xFe_{2-y}Se_2$. *Phys. Rev. B* **83**, 060512(R) (2011).
3. M. Burrard-Lucas, D. G. Free, S. J. Sedlmaier, J. D. Wright, S. J. Cassidy, Y. Hara, A. J. Corkett, T. Lancaster, P. J. Baker, S. J. Blundell, S. J. Clarke, Enhancement of the superconducting transition temperature of FeSe by intercalation of a molecular spacer layer. *Nat. Mater.* **12**, 15–19 (2013).
4. X. F. Lu, N. Z. Wang, H. Wu, Y. P. Wu, D. Zhao, X. Z. Zeng, X. G. Luo, T. Wu, W. Bao, G. H. Zhang, F. Q. Huang, Q. Z. Huang, X. H. Chen, Coexistence of superconductivity and antiferromagnetism in $(Li_{0.8}Fe_{0.2})OHFeSe$. *Nat. Mater.* **14**, 325–329 (2015).
5. Q.-Y. Wang, Z. Li, W.-H. Zhang, Z.-C. Zhang, J.-S. Zhang, W. Li, H. Ding, Y.-B. Ou, P. Deng, K. Chang, J. Wen, C.-L. Song, K. He, J.-F. Jia, S.-H. Ji, Y.-Y. Wang, L.-L. Wang, X. Chen, X.-C. Ma, Q.-K. Xue, Interface-induced high-temperature superconductivity in single unit-cell FeSe films on $SrTiO_3$. *Chin. Phys. Lett.* **29**, 037402 (2012).
6. Y. Miyata, K. Nakayama, K. Sugawara, T. Sato, T. Takahashi, High-temperature superconductivity in potassium coated multilayer FeSe thin films. *Nat. Mater.* **14**, 775–780 (2015).
7. K. Hanzawa, H. Sato, H. Hiramatsu, T. Kamiya, H. Hosonoa, Electric field-induced superconducting transition of insulating FeSe thin film at 35 K. *Proc. Natl. Acad. Sci. U.S.A.* **113**, 3986–3990 (2016).
8. B. Lei, J. H. Cui, Z. J. Xiang, C. Shang, N. Z. Wang, G. J. Ye, X. G. Luo, T. Wu, Z. Sun, X. H. Chen, Evolution of high-temperature superconductivity from a low-T_c phase tuned by carrier concentration in FeSe thin flakes. *Phys. Rev. Lett.* **116**, 077002 (2016).
9. J. Shiogai, Y. Ito, T. Mitsuhashi, T. Nojima, A. Tsukazaki, Electric-field-induced superconductivity in electrochemically etched ultrathin FeSe films on $SrTiO_3$ and MgO. *Nat. Phys.* **12**, 42–46 (2016).
10. Y. Zhang, L. X. Yang, M. Xu, Z. R. Ye, F. Chen, C. He, H. C. Xu, J. Jiang, B. P. Xie, J. J. Ying, X. F. Wang, X. H. Chen, J. P. Hu, M. Matsunami, S. Kimura, D. L. Feng, Nodeless superconducting gap in $A_xFe_2Se_2$ (A=K, Cs) revealed by angle-resolved photoemission spectroscopy. *Nat. Mater.* **10**, 273–277 (2011).
11. D. Liu, W. Zhang, D. Mou, J. He, Y.-B. Ou, Q.-Y. Wang, Z. Li, L. Wang, L. Zhao, S. L. He, Y. Peng, X. Liu, C. Chen, L. Yu, G. Liu, X. Dong, J. Zhang, C. Chen, Z. Xu, J. Hu, X. Chen,

X. Ma, Q. Xue, X. Zhou, Electronic origin of high-temperature superconductivity in single-layer FeSe superconductor. *Nat. Commun.* **3**, 931 (2012).
12. S. Tan, Y. Zhang, M. Xia, Z. Ye, F. Chen, X. Xie, R. Peng, D. Xu, Q. Fan, H. Xu, J. Jiang, T. Zhang, X. Lai, T. Xiang, J. Hu, B. Xie, D. Feng, Interface-induced superconductivity and strain-dependent spin density waves in FeSe/$SrTiO_3$ thin films. *Nat. Mater.* **12**, 634–640 (2013).
13. X. H. Niu, R. Peng, H. C. Xu, Y. J. Yan, J. Jiang, D. F. Xu, T. L. Yu, Q. Song, Z. C. Huang, Y. X. Wang, B. P. Xie, X. F. Lu, N. Z. Wang, X. H. Chen, Z. Sun, D. L. Feng, Surface electronic structure and isotropic superconducting gap in ($Li_{0.8}Fe_{0.2}$)OHFeSe. *Phys. Rev. B* **92**, 060504(R) (2015).
14. L. Zhao, A. Liang, D. Yuan, Y. Hu, D. Liu, J. Huang, S. He, B. Shen, Y. Xu, X. Liu, L. Yu, G. Liu, H. Zhou, Y. Huang, X. Dong, F. Zhou, K. Liu, Z. Lu, Z. Zhao, C. Chen, Z. Xu, X. J. Zhou, Common electronic origin of superconductivity in (Li,Fe)OHFeSe bulk superconductor and single-layer FeSe/$SrTiO_3$ films. *Nat. Commun.* **7**, 10608 (2016).
15. Q. Fan, W. H. Zhang, X. Liu, Y. J. Yan, M. Q. Ren, R. Peng, H. C. Xu, B. P. Xie, J. P. Hu, T. Zhang, D. L. Feng, Plain *s*-wave superconductivity in single-layer FeSe on $SrTiO_3$ probed by scanning tunnelling microscopy. *Nat. Phys.* **11**, 946–952 (2015).
16. Y. J. Yan, W. H. Zhang, M. Q. Ren, X. Liu, X. F. Lu, N. Z. Wang, X. H. Niu, Q. Fan, J. Miao, R. Tao, B. P. Xie, X. H. Chen, T. Zhang, D. L. Feng, Surface electronic structure and evidence of plain *s*-wave superconductivity in ($Li_{0.8}Fe_{0.2}$)OHFeSe. *Phys. Rev. B* **94**, 134502 (2016).
17. C.-L. Song, Y.-L. Wang, P. Cheng, Y.-P. Jiang, W. Li, T. Zhang, Z. Li, K. He, L. L. Wang, J.-F. Jia, H.-H. Hung, C. Wu, X. Ma, X. Chen, Q.-K. Xue, Direct observation of nodes and twofold symmetry in FeSe superconductor. *Science* **332**, 1410–1413 (2011).
18. T. Hanaguri, S. Niitaka, K. Kuroki, H. Takagi, Unconventional *s*-wave superconductivity in Fe(Se,Te). *Science* **328**, 474–476 (2010).
19. C.-L. Song, H.-M. Zhang, Y. Zhong, X.-P. Hu, S.-H. Ji, L. Wang, K. He, X.-C. Ma, Q.-K. Xue, Observation of double-dome superconductivity in potassium-doped FeSe thin films. *Phys. Rev. Lett.* **116**, 157001 (2016).
20. C. H. P. Wen, H. C. Xu, C. Chen, Z. C. Huang, X. Lou, Y. J. Pu, Q. Song, B. P. Xie, M. Abdel-Hafiez, D. A. Chareev, A. N. Vasiliev, R. Peng, D. L. Feng, Anomalous correlation effects and unique phase diagram of electron-doped FeSe revealed by photoemission spectroscopy. *Nat. Commun.* **7**, 10840 (2016).
21. X. Dong, K. Jin, D. Yuan, H. Zhou, J. Yuan, Y. Huang, W. Hua, J. Sun, P. Zheng, W. Hu, Y. Mao, M. Ma, G. Zhang, F. Zhou, Z. Zhao, ($Li_{0.84}Fe_{0.16}$)$OHFe_{0.98}Se$ superconductor: Ion-exchange synthesis of large single-crystal and highly two-dimensional electron properties. *Phys. Rev. B* **92**, 064515 (2015).
22. Z. Du, X. Yang, H. Lin, D. Fang, G. Du, J. Xing, H. Yang, X. Zhu, H.-H. Wen, Scrutinizing the double superconducting gaps and strong coupling pairing in ($Li_{1-x}Fe_x$)OHFeSe. *Nat. Commun.* **7**, 10565 (2016).
23. Y. Zhang, J. J. Lee, R. G. Moore, W. Li, M. Yi, M. Hashimoto, D. H. Lu, T. P. Devereaux, D.-H. Lee, Z.-X. Shen, Superconducting gap anisotropy in monolayer FeSe thin film. *Phys. Rev. Lett.* **117**, 117001 (2016).
24. D. Huang, C.-L. Song, T. A. Webb, S. Fang, C.-Z. Chang, J. S. Moodera, E. Kaxiras, J. E. Hoffman, Revealing the empty-state electronic structure of single-unit-cell FeSe/$SrTiO_3$. *Phys. Rev. Lett.* **115**, 017002 (2015).
25. F. W. Zheng, L.-L. Wang, Q.-K. Xue, P. Zhang, Band structure and charge doping effects of the potassium-adsorbed FeSe/$SrTiO_3$ system. *Phys. Rev. B* **93**, 075428 (2016).
26. B. Lei, Z. J. Xiang, X. F. Lu, N. Z. Wang, J. R. Chang, C. Shang, A. M. Zhang, Q. M. Zhang, X. G. Luo, T. Wu, Z. Sun, X. H. Chen, Gate-tuned superconductor-insulator transition in (Li,Fe)OHFeSe. *Phys. Rev. B* **93**, 060501(R) (2016).
27. R. Khasanov, H. Zhou, A. Amato, Z. Guguchia, E. Morenzoni, X. Dong, G. Zhang, Z. Zhao, Proximity-induced superconductivity within the insulating ($Li_{0.84}Fe_{0.16}$)OH layers in ($Li_{0.84}Fe_{0.16}$)$OHFe_{0.98}Se$. *Phys. Rev. B* **93**, 224512 (2016).
28. I. I. Mazin, D. J. Singh, M. D. Johannes, M. H. Du, Unconventional superconductivity with a sign reversal in the order parameter of $LaFeAsO_{1-x}F_x$. *Phys. Rev. Lett.* **101**, 057003 (2008).
29. P. J. Hirschfeld, M. M. Korshunov, I. I. Mazin, Gap symmetry and structure of Fe-based superconductors. *Rep. Prog. Phys.* **74**, 124508 (2011).
30. F. Wang, F. Yang, M. Gao, Z.-Y. Lu, T. Xiang, D.-H. Lee, The electron pairing of $K_xFe_{2-y}Se_2$. *Europhys. Lett.* **93**, 57003 (2011).
31. T. A. Maier, S. Graser, P. J. Hirschfeld, D. J. Scalapino, *d*-wave pairing from spin fluctuations in the $K_xFe_{2-y}Se_2$ superconductors. *Phys. Rev. B* **83**, 100515 (2011).
32. Y. Bang, A shadow gap in the over-doped ($Ba_{1-x}K_x$)Fe_2As_2 compound. *New J. Phys.* **16**, 023029 (2014).
33. X. Chen, S. Maiti, A. Linscheid, P. J. Hirschfeld, Electron pairing in the presence of incipient bands in iron-based superconductors. *Phys. Rev. B* **92**, 224514 (2015).
34. A. Linscheid, S. Maiti, Y. Wang, S. Johnston, P. J. Hirschfeld, High T_c via spin fluctuations from incipient bands: Application to monolayers and intercalates of FeSe. *Phys. Rev. Lett.* **117**, 077003 (2016)
35. H. Miao, T. Qian, X. Shi, P. Richard, T. K. Kim, M. Hoesch, L. Y. Xing, X.-C. Wang, C.-Q. Jin, J.-P. Hu, H. Ding, Observation of strong electron pairing on bands without Fermi surfaces in $LiFe_{1-x}Co_xAs$. *Nat. Commun.* **6**, 6056 (2015).
36. N. Arakawa, M. Ogata, Orbital-selective superconductivity and the effect of lattice distortion in iron based superconductors. *J. Phys. Soc. Jpn.* **80**, 074704 (2011).
37. A. Kreisel, B. M. Andersen, P. O. Sprau, A. Kostin, J. C. S. Davis, P. J. Hirschfeld, Orbital selective pairing and gap structures of iron-based superconductors. *arXiv:1611.02643* (2016).
38. P. O. Sprau, A. Kostin, A. Kreisel, A. E. Böhmer, V. Taufour, P. C. Canfield, S. Mukherjee, P. J. Hirschfeld, B. M. Andersen, J. C. S. Davis, Discovery of orbital-selective cooper pairing in FeSe. *arXiv:1611.02134* (2016).
39. M. Imada, A. Fujimori, Y. Tokura, Metal-insulator transitions. *Rev. Mod. Phys.* **70**, 1039–1263 (1998).
40. X. H. Niu, S. D. Chen, J. Jiang, Z. R. Ye, T. L. Yu, D. F. Xu, M. Xu, Y. Feng, Y. J. Yan, B. P. Xie, J. Zhao, D. C. Gu, L. L. Sun, Q. Mao, H. Wang, M. Fang, C. J. Zhang, J. P. Hu, Z. Sun, D. L. Feng, A unifying phase diagram with correlation-driven superconductor-to-insulator transition for the 122 series of iron chalcogenides. *Phys. Rev. B* **93**, 054516 (2016).
41. X. Wu, S. Qin, Y. Liang, H. Fan, J. Hu, Topological characters in $Fe(Te_{1-x}Se_x)$ thin films. *Phys. Rev. B* **93**, 115129 (2016).
42. X. Shi, Z.-Q. Han, X.-L. Peng, P. Richard, T. Qian, X.-X. Wu, M.-W. Qiu, S. C. Wang, J. P. Hu, Y.-J. Sun, H. Ding, Enhanced superconductivity accompanying a Lifshitz transition in electron-doped FeSe monolayer. *Nat. Commun.* **8**, 14988 (2017).

Acknowledgments: We thank D. C. Peets and B. Y. Pan for helpful discussions. **Funding:** This work was supported by the National Science Foundation of China and National Key R&D Program of the Ministry of Science and Technology of China (grant nos. 2016YFA0300200 and 2017YFA0303004) and Science Challenge Project (grant no. TZ2016004). **Author contributions:** M.Q.R., Y.J.Y., and R.T. performed the STM/STS measurement and analyzed the data. X.H.N. and R.P. performed the ARPES measurement and analyzed the data. D.H. synthesized the sample under the guidance of J.Z. T.Z. and D.-L.F. designed and coordinated the whole work and wrote the manuscript. All authors have discussed the results and the interpretation. **Competing interests:** The authors declare that they have no competing interests. **Data and materials availability:** All data needed to evaluate the conclusions in the paper are present in the paper and/or the Supplementary Materials. Additional data related to this paper may be requested from the authors.

Submitted 21 December 2016
Accepted 26 May 2017
Published 14 July 2017
10.1126/sciadv.1603238

Citation: M. Ren, Y. Yan, X. Niu, R. Tao, D. Hu, R. Peng, B. Xie, J. Zhao, T. Zhang, D.-L. Feng, Superconductivity across Lifshitz transition and anomalous insulating state in surface K–dosed ($Li_{0.8}Fe_{0.2}$OH)FeSe. *Sci. Adv.* **3**, e1603238 (2017).

Science Advances

Superconductivity across Lifshitz transition and anomalous insulating state in surface K–dosed ($Li_{0.8}Fe_{0.2}OH$)FeSe

Mingqiang Ren, Yajun Yan, Xiaohai Niu, Ran Tao, Die Hu, Rui Peng, Binping Xie, Jun Zhao, Tong Zhang and Dong-Lai Feng

Sci Adv **3** (7), e1603238.
DOI: 10.1126/sciadv.1603238